Proceedings of ISFOG 2025
5TH INTERNATIONAL SYMPOSIUM ON
FRONTIERS IN OFFSHORE GEOTECHNICS
Nantes, France | June 9-13 2025

ISBN 978-2-85782-758-0

The yield strength and compressibility of glauconitic sands in the U.S. Atlantic Outer Continental Shelf

P. Peralta*, K. Vembu, and S. Esmailzadeh
Fugro USA Marine, Inc., Norfolk, U.S.

p.peralta@fugro.com (corresponding author)

ABSTRACT: Glauconitic soils have recently come into focus as thick layers of glauconite-rich deposits have been encountered during site characterization of several offshore wind farm lease areas in the U.S. Atlantic Coast. Glauconite particles in its undisturbed state are weaker than silica quartz sand particles and are generally crushable, leading to high compressibility and soil strength degradation under large and repeated loads such as what would be encountered for structures in the marine environment. This paper focuses on the yield strength and compressibility behavior of glauconitic sands with varying amounts of glauconite particles as can be found in the U.S. Atlantic Coast. A series of one-dimensional compression tests performed on glauconitic sands were analyzed to examine particle strength and the onset of particle damage and crushing as the vertical stress increases, and its effect on the yield stress and primary compression. The particle damage occurring in glauconitic sands and its effect on soil compressibility is compared to published results for silica quartz sands and other compressible soils such as carbonate soils.

Keywords: Glauconite; Compressibility, Grain Crushing, Yield Strength

1 BACKGROUND

The U.S. Atlantic outer continental shelf (OCS) has seen the development of several offshore wind lease areas in the last decade. The ensuing surveys and site investigations have identified glauconite formations at several of the offshore wind farm lease areas. Glauconite is an iron potassium phyllosilicate mineral that occurs most characteristically in round, pellet form with grain size varying from 1/30 mm in diameter to a little over 1 mm, and hence are typically classified as “sands”. Its name is derived from the Greek word “glaukonit”, which alludes to its greenish-blue hue.

Glauconite is widely distributed and known to form on all continental shelfs; however, the low-subsidence rate margin at the Atlantic OCS make it conducive to the formation of thick glauconite-rich sequences. Glauconite typically has a Mohs scale hardness of 2 and thus lower resistance to particle abrasion, fracturing and weathering compared to silica sands, which has a Mohs scale hardness of 7. The low hardness of glauconite minerals is indicative of its potential for particle damage and grain crushing at lower stress levels and thus higher compressibility of the soil aggregate.

This study investigates the compressibility behavior and the stress levels leading to onset of particle damage and grain crushing of aggregate sands with varying concentrations of glauconite under 1D laterally constrained compression loading.

2 U.S. ATLANTIC SHELF GEOLOGY

The U.S. Atlantic OCS geology was significantly influenced by the glacial and interglacial cycles during the Quaternary period with the last two major glacial events, the Wisconsinan and the Illinoian shaping the present-day sequence of Holocene and Pleistocene sediments. The U.S. Atlantic is a low subsidence-rate margin and is more subject to the variations of sea level (Harris & Whiting, 2000). The sequence of Holocene and Pleistocene sediments is generally 10 m to 60 m thick throughout most of the shelf (Emery and Uchupi, 1984) and unconformably overlie older Pre-Quaternary coastal plain deposits.

Glauconite-rich intervals, which are generally formed during periods of low sedimentation rates, have been found to be present along the U.S. Atlantic margin and are thought to have formed within a lowstand systems tract and within a transgressive systems tract. However, glauconite may form in many depositional settings, such as maximum flooding surfaces, incised valley fill, shelf margin wedges, etc. The Plio-Pleistocene appears to be the upper limit of glauconite-rich formation offshore within the U.S. Atlantic margin (Amorosi, 1997; Harris & Whiting, 2000).

3 GLAUCONY MINERAL

Several authors have described the characteristics of glauconite and its geological background (Amorosi, 1997; Westgate et al, 2022, others). A brief description and summary are provided here. Glauconite is a mineral rich in potassium and iron that typically forms as rounded aggregates or pellets, varying in color from light green to dark green or black, depending on its maturity. Glaucony minerals can form through two primary processes: allogenic and authigenic.

Authigenic glaucony forms in situ within sedimentary environments under low sedimentation rates and sub-oxic conditions. The glauconization process begins with the precipitation of a potassium- (K) and iron- (Fe) poor glauconitic-smectite within precursor substrate grains, forming light green grains with low potassium oxide (K_2O) content (2 to 4%). Over longer periods (10^2 to 10^6 years), glauconitic-smectite evolves chemically through ionic exchange with seawater and porewaters, incorporating Fe^{2+} and K^+ while losing aluminum (Al). This results in the formation of glauconite-mica, characterized by dark green grains with a smooth appearance and higher K_2O content (4 to 6%) (Meunier and Albani, 2007). In its mature, highly evolved state, glaucony can exceed 8% K_2O.

Allogenic glaucony originates from the physical transport and redeposition of glauconitic grains formed elsewhere, often via rivers, currents, storms, or bioturbation. Transport leads to abrasion or even disaggregation of glauconitic sands creating glauconitic fines, with resulting grains exhibiting varying degrees of maturity based on the extent of glauconitization prior to transport and subsequent chemical alteration

4 SUMMARY OF TESTS PERFORMED

Soil classification, minerology and 1-D compression (oedometer) tests were reviewed in this study to investigate the mechanical behavior of quartz sands with glauconite particles under 1D compression. The tests were performed on mainly silica quartz sand samples with varying amounts of glauconite that were acquired from several sites along the U.S. Atlantic OCS.

In this study, the test results from a total of 10 sand samples were analyzed. The samples generally consist of silica quartz sand with glauconite content ranging from 0% to 90%. The sand samples were retrieved through downhole boring and preserved in quart containers in an undisturbed state. At some borehole locations where the sand samples were retrieved, cone penetration tests (CPT) were paired and performed adjacent to the samples. The paired CPT data are presented for each sand sample investigated. The list of sand samples that were investigated in this study, their minerology and angularity, as well as relative density D_r and CPT cone tip resistance, q_c (kPa), and friction ratio, R_F, is provided in Table 1.

4.1 Description of Minerology Tests

Soil mineralogy and angularity of the sand samples were determined from microphotographs taken by a digital camera attached on a Meiji EMZ—TR (7x—4.5x) Trinocular microscope system. A small amount of soil was spread in a 25 mm to 30 mm diameter circle of sediment on a smear plate for microscopic inspection. Photographs were captured on soil specimens in original state and after being washed on a 63 μm sieve. Mineral components were determined by visual (qualitative) assessment of the grains. Soil particles roundness and sphericity determination were based on the shape determination chart modified from Krumbein and Sloss (1963).

4.2 Description of Oedometer Tests

1D laterally constrained compression tests under incremental loading (IL) conditions were performed on all samples investigated in this study. The compression tests were performed on undisturbed samples or samples reconstituted to their estimated in situ relative density (Table 1). Each test specimen was prepared using a stainless-steel ring with 60 to 64 mm inside diameter and 20 to 25 mm height. The test specimens were loaded to the maximum vertical pressures allowed by the load frame, which was approximately 25 MPa. The loading schedule included one unloading-reloading loop. The specimens were loaded to the situ conditions and unloaded to very low stress levels before reloading again.

5 GRAIN CRUSHING

5.1 Particle Damage and Crushing Level

Under 1D and isotropic compression tests of granular soil, increasing levels of particle damage or crushing occurs as the effective vertical stress σ'_v increases. Several authors have categorized particle damage and grain crushing of granular material into three levels (Hardin, 1985, Pestana and Whittle, 1995; Mesri and Vardhanabhuti, 2009; others):

Table 1. Summary of soil composition and properties of sand samples investigated in this study.

Sample No.	Minerology	Angularity	$D50$ (mm)	D_r [%]	q_C [MPa]	R_F [-]
S-1	0% glauconite, 98% quartz, 2% dark opaque	Subrounded to well rounded	0.23	75	40	~0.5
S-2	2% glauconite, 90% quartz, 2% dark opaque, 1% lithic fragments	subangular to well rounded	0.21	100	68	~0.5
S-3	10% glauconite, 90% quartz	angular to rounded	0.24	100	61	~1.0
S-4	10% glauconite, 88% quartz, 2% shell	subangular to rounded	0.84	55	NA	NA
S-5	18% glauconite, 79% quartz, 2% lithic fragments, 1% shell fragments	subangular to rounded	0.25	85	49	~1.0
S-6	55% glauconite, 45% quartz	subrounded to well rounded	0.20	60	28	~6.0
S-7	65% glauconite, 5% quartz, 30% fines	subrounded to well rounded	0.19	55	18	~8.0
S-8	75% glauconite, 10% quartz, 15% fines	subangular to subrounded	0.29	60	22	~8.5
S-9	85% glauconite, 10% fines, 5% shell fragments	subrounded to well rounded	0.22	45	19	~8.0
S-10	90% glauconite, 10% quartz	subrounded to wellr ounded	0.18	60	33	~9.0

Notes:
D50 – Mean grain size
D_r – Relative density interpreted from cone penetration resistance.
q_C – Cone penetration resistance.
R_F – Friction ratio.

- Particle damage level I – abrasion or grinding of grain surface asperities.
- Particle damage level II – crushing and/or breaking of grain surface protrusions.
- Particle damage level III – crushing, fracturing, splitting and/or shattering of the grain.

The yield stress at the maximum curvature, $\sigma'_{v,MC}$, of the void ratio e vs $\log \sigma'_v$ plot from 1D compression tests traditionally defines the stress level that marks the abrupt onset of increased compressibility. For clayey/silty soils, the yield stress is the preconsolidation pressure and defines the boundary between the recompression and virgin compression lines. In granular material, the onset of increased compressibility is thought to be due to particle damage and associated particle rearrangement (McDowell and Bolton, 1998; Mesri and Vardhanabhuti, 2009; others). Mesri and Vardhanabhuti (2009) studied the compression behavior of 104 mainly silica and carbonate sands and observed 3 types of compression behavior linked to the level of particle damage, described in the following.

5.1.1 Hard Granular Material

In most granular material with a high degree of hardness and coarse particles, e.g. clean and well-rounded quartz silica sands, the e - σ'_v plot exhibits 3 stages, which mark the onset of increasing levels of damage to the particles. In stage (1), level I and II particle damage occur at low stress levels leading to improved packing and interparticle contact of the grains and an increase in the constrained modulus M (defined as the ratio of change in effective vertical stress $\Delta\sigma'_v$ to change in vertical strain $\Delta\varepsilon_v$). In stage (2), as the vertical stress increases, major particle fracturing and crushing occurs (level III particle damage) leading to collapse of the soil aggregate and hence, an abrupt decrease in the constrained modulus M. In stage (3) of the compression curve, at increasingly high levels of applied vertical stress, major particle fracturing essentially completes and there is an improved packing of the fractured particles and an increase in M. The yield stresses $\sigma'_{v,Mmax}$ and $\sigma'_{v,Mmin}$ correspond to the inflection points on the e vs σ'_v plot marking the onset of stage (2) and stage (3) compression, respectively.

5.1.2 Weak Granular Material

In weaker granular soils, e.g. micaceous or carbonate sands, no distinct stages could be observed in the compression curves. Significant level I and II particle damage occurs and level III particle damage gradually begins at low vertical stress levels and continues throughout compression. All 3 levels of particle damage under increasing stress levels lead to improved gradation and packing of the particles with the constrained modulus M continuously increasing. For

this type of compression behavior, no inflection points (yield stresses $\sigma'_{v,Mmax}$ and $\sigma'_{v,Mmin}$) in the e vs σ'_v plot could be observed to mark the onset of particle damage. However, the yield stress at maximum curvature $\sigma'_{v,MC}$ from the e vs $\log \sigma'_v$ plot can be used to identify the onset of increased compression.

5.1.3 Transitional Granular Material

For transitional soils with intermediate hardness (between hard and weak granular material) Mesri and Vardhanabhuti (2009) observed 3 stages of compression, similar to the case of strong or hard granular soils, but the constrained modulus M never decreases throughout compression, similar to the case of weak granular soils. In stage (1) at low stress levels, level I and II particle damage occur leading to improved packing, which can be observed from the gradual increase in M. In stage (2) of the compression curve, level III particle damage begins. However, the improved packing and interparticle contact from level I and II particle damage balances with the large interparticle movements under major particle fracturing, so M remains contant. Stage (3) is marked by the gradual increase in M as the process of major particle fracturing (level III damage) completes.

5.2 Comparison of 1D Compressibility

The e vs σ'_v and e vs $\log \sigma'_v$ plots from 1D compression tests of the glauconitic sand samples listed in Table 1 and Table 2 were reviewed to compare against the compressibility behavior types outlined by Mesri and Vardhanabhuti (2009), and to identify the range of effective vertical stresses that marks the onset of particle damage levels I, II and III in glauconitic sands, i.e., $\sigma'_{v,Mmax}$ and $\sigma'_{v,MC}$.

Figure 1 shows the compression curves for quartz sand samples with less than 20 % glauconite, while Figure 2 illustrates the compression curves for quartz sand samples with more than 50 % glauconite.

The effective vertical stress level marking the onset of level III particle damage, $\sigma'_{v,Mmax}$, was estimated from the change in constrained modulus M on the e vs σ'_v plots. For comparison, the effective vertical stress level marking the onset of increased compression, $\sigma'_{v,MC}$, was also determined from the maximum curvature point on the e vs $\log \sigma'_v$ plots.

Table 2 shows the observed stress levels at which level III particle damage and/or increased compression begins to occur for the sand samples tested in this study.

Table 2. Vertical effective stress level at which grain crushing (level III particle damage) begins.

Sand Sample No.	Percent Glauconite [%]	$\sigma'_{v,MC}$ [kPa]	$\sigma'_{v,Mmax}$ [kPa]	$\frac{\sigma'_{v,MC}}{\sigma'_{v,Mmax}}$
1	0	3064	2800	1.1
2	2	4410	6129	0.7
3	10	4410	3064	1.4
4	10	2378	2880	0.8
5	18	4620	3064	1.5
6	55	3653	2000	1.8
7	65	2920	1460	2.0
8	75	3315	2000	1.7
9	85	3165	2000	1.6
10	90	2000	1000	2.0

The yield stress $\sigma'_{v,Mmax}$ was observed to range from ~ 2.8 MPa to 6 MPa for the sand samples with glauconite content between 0% and 18% and from ~ 1 MPa to 2 MPa for the sand samples with glauconite content between 55% and 90%.

The ratio of $\sigma'_{v,MC}$ to $\sigma'_{v,Mmax}$ was observed to range from 0.7 to 1.8. Mesri and Vardhanabhuti (2009) observed that $\sigma'_{v,Mmax}$, taken from a database of 57 sands, may range from 0.3 MPa for angular carbonate sands to ~30 MPa for well-rounded purely silica quartz sands. And the ratio of $\sigma'_{v,MC}$ to $\sigma'_{v,Mmax}$ was observed to range from 0.7 to 2.5. The ratio of yield stresses and the $\sigma'_{v,Mmax}$ values for the glauconitic sand samples generally agree very well with the above authors' results from a larger database, as compared and presented in Figure 3.

Figure 4 re-plots the compressibility curves presented in Mesri and Vardhanabhuti (2009), which shows the range of compression index C_c versus $\log \sigma'_v$ curves and the range of observed yield stress at maximum curvature, $\sigma'_{v,MC}$, for 3 groups of sands (loose to very dense quartz sands, quarz sands with 10% to 20% fines, and carbonate sands). The compressibility curves presented in Mesri and Vardhanabhuti (2009) illustrate the higher compressibility and lower yield stress levels, and therefore earlier onset of particle crushing, of quartz sands with fines and carbonate sands compared to clean, quartz sands. The C_c versus $\log \sigma'_v$ curves for the glauconitic sand samples in this study are also presented in Figure 4. It can be observed that the compressibility behavior of sand samples with less than 20% glauconite is similar to that of clean, quartz sand.

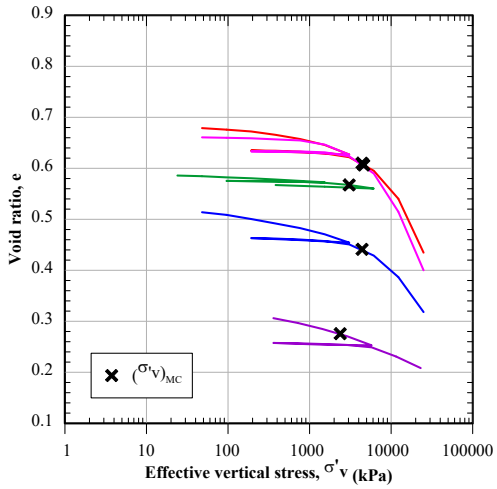

(a)

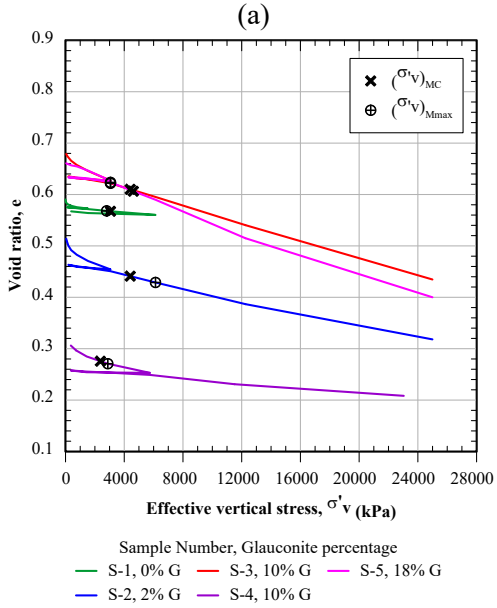

(b)

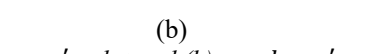

Figure 1. (a) e vs σ'_v plot and (b) e vs log σ'_v plot showing onset of levels I, II, and III particle damage of silica quartz sands with < 20% glauconite particles.

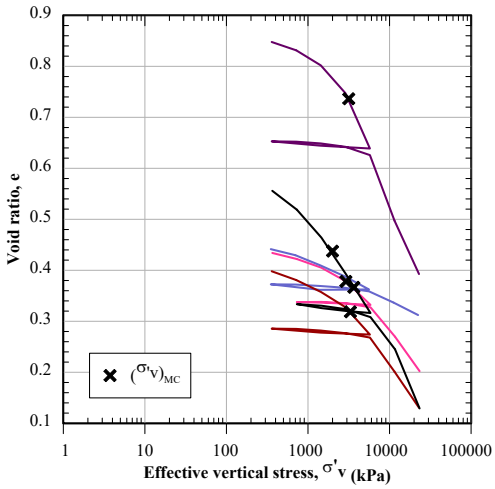

(a)

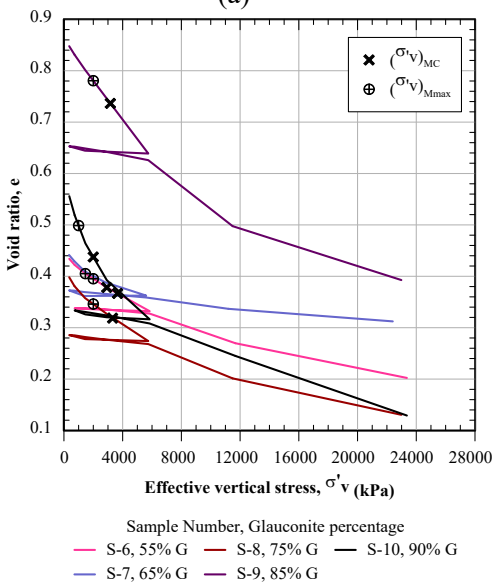

(b)

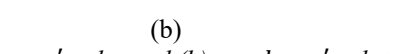

Figure 2. (a) e vs σ'_v plot and (b) e vs log σ'_v plot showing onset of levels I, II, and III particle damage of silica quartz sands with > 50% glauconite particles.

The compressibility behavior of sand samples with more than 50% glauconite is similar to quartz sands with 10% to 20% fines and less compressible than carbonate sands. The range of the yield stress $\sigma'_{v,MC}$ for the glauconitic sand samples is between the range of yield stress for carbonate sands and clean, quartz sands.

6 CONCLUSIONS

The compressibility behavior, compression index, and yield stresses signaling the onset of particle damage for 10 silica quartz sand samples with varying amounts of glauconite are presented in this study.

The results are compared to data for clean, quartz sands to carbonate sands from Mesri and Vardhanabhuti (2009). The results of this study show that the yield stress marking the onset of major particle fracturing and crushing (level III particle damage), $\sigma'_{v,Mmax}$, is between 2.8 MPa to 6 MPa for the sand samples with glauconite content between 0% and 18%.

Lower values of $\sigma'_{v,Mmax}$ ranging from ~ 1 MPa to 2 MPa were observed for the sand samples with glauconite content between 55% and 90%. Furthermore, the compressibility behavior of the sand samples with glauconite content between 0% and 18% was observed to be similar to clean, quartz sands, while the compressibility behavior of the sand samples with glauconite content between 55% and 90% was similar to quartz sands with fines.

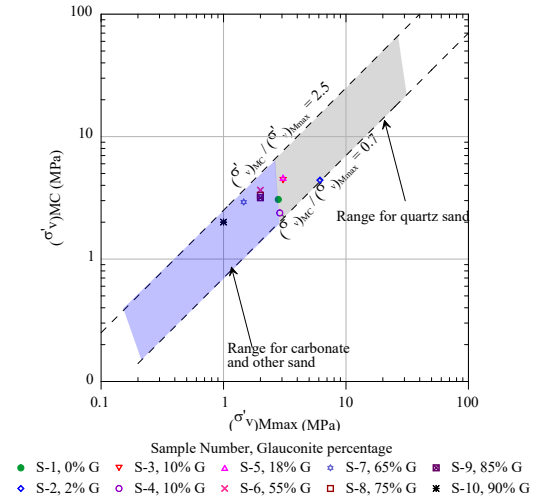

Figure 3. Comparison of $(\sigma'_v)_{Mmax}$ for glauconitic sand samples in this study and 42 quartz to carbonate sands in Mesri and Vardhanabhuti (2009).

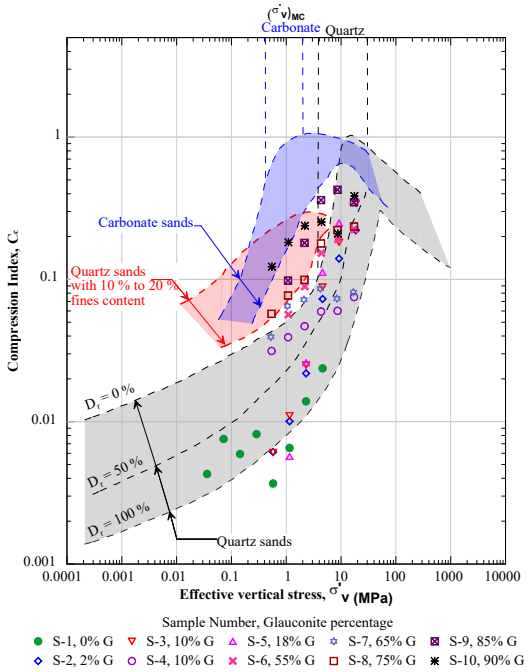

Figure 4. Comparison of compressibility index of glauconitic sands in this study with clean, quartz sands to carbonate sands in Mesri and Vardhanabhuti (2009).

The sand samples with higher glauconite content up to 90% were less compressible than the carbonate sands. The range of values of the yield stress marking abrupt or increased compressibility, $\sigma'_{v,MC}$, for the glauconitic samples can be observed to be between the range of yield stresses for carbonate sands and for clean, quartz sands. The yield stresses from this study provide an indication of the particle strength and resistance to fracturing and crushing of silica sands with glauconite content ranging from 0% to 90%, which are typical for the Atlantic OCS sediments. The results have implications on modelling the behavior of glauconitic sands under high compression loads for foundation engineering analyses.

AUTHOR CONTRIBUTION STATEMENT

Proserpine Peralta: Conceptualization, Writing- Original draft, Reviewing and Editing. **Kalaiarasi Vembu**: Data curation, Validation, Formal Analysis, **Saba Esmailzadeh**: Writing- Reviewing and Editing.

REFERENCES

Amorosi, A. (1997). Detecting compositional, spatial, and temporal attributes of glaucony: a tool for provenance research. Sedimentary Geology, 109, 135-153. https://doi.org/10.1016/S0037-0738(96)00042-5.

Emery, K.O. & Uchupi, E. (1984). The Geology of the Atlantic Ocean. Springer-verlag.

Hardin, B.O. (1985). Crushing of soil particles. Journal of Geotechnical and Geoenvironmental Engineering, ASCE, 10, 1177-1792. https://doi.org/10.1061/(ASCE)0733-9410(1985)111:10(1177.

Harris, L.C. & Whiting, B.M. (2000). Sequence-stratigraphic significance of Miocene to Pliocene glauconite-rich layers, on- and offshore of the US Mid-Atlantic margin. Sedimentary Geology 134 (2000), 129-147. https://doi.org/10.1016/S0037-0738(00)00017-8.

Krumbein, W. C., & Sloss, L. (1963). Stratigraphy and sedimentation (2nd ed.). W. H. Freeman and Co. San Francisco.

McDowell, G.R. & Bolton, M.D. (1998). On the micromechanics of crushable aggregates. Geotechnique, 48. 667-679. https://doi.org/10.1680/geot.1998.48.5.667.

Mesri, G., & Vardhanabhuti, B. (2009). Compression of granular materials. Canadian Geotechnical Journal, 46(4), 369-392. https://doi.org/10.1139/T08-12.

Meunier, A., & El Albani, A. (2007). The glauconite–Fe-illite–Fe-smectite problem: a critical review. Terra Nova, 19, 95-104. https://doi.org/10.1111/j.1365-3121.2006.00719.x.

Pestana, J.M. & Whittle, A.J. (1995). Compression model for cohesionless soils. Geotechnique, 45, 611-631. https://doi.org/10.1680/geot.1995.45.4.611.

Westgate, Z., McMullin, C., Zepipilli, D., Beemer, R., & DeGroot, D. (2022). Geological and Geotechnical Characteristics of Glauconitic Sands. Geoc-Congress 2022 GSP 333, 113-121. https://doi.org/10.1061/9780784484036.012.